Hindawi Publishing Corporation
International Journal of Photoenergy
Volume 2008, Article ID 631597, 8 pages
doi:10.1155/2008/631597

*Research Article*

# Electrochemical Investigation of Doped Titanium Dioxide

**J. W. J. Hamilton,[1] J. A. Byrne,[1] C. McCullagh,[2] and P. S. M. Dunlop[1]**

[1] *Nanotechnology and Integrated BioEngineering Centre (NIBEC), University of Ulster, Jordanstown Campus, Newtownabbey, County Antrim BT37 0QB, Northern Ireland, UK*
[2] *The School of Resources and Environment Engineering (CREE), Faculty of Design and Technology, The Robert Gordon University, Clarke Building, Schoolhill, Aberdeen, AB10 1FR, UK*

Correspondence should be addressed to J. W. J. Hamilton, jwj.hamilton@ulster.ac.uk

Received 30 August 2007; Revised 7 January 2008; Accepted 25 January 2008

Recommended by Vincenzo Augugliaro

Thin films of transition-metal doped (0.2, 1.0, and 5.0 atom%) $TiO_2$ were prepared on titanium foil using a sol-gel route catalyzed by ammonium acetate. Dopants investigated were the fourth-period transition metals. The prepared films were characterised by Raman spectroscopy, Auger electron spectroscopy, and photoelectrochemical methods. The films doped with transition metals showed a lower photocurrent response than undoped samples. No major red shift in the photocurrent response spectra of the doped films was observed. A photocurrent response was observed under visible light irradiation of the samples and was potential dependent peaking around −0.3 V (SCE), which is indicative of electron promotion from a filled defect level. Examination of the defect level potential dependence by analysis of the current-time response under chopped illumination at fixed potential (−0.8 V–+1.07 V) gave a good correlation with the potential dependence observed in the visible light irradiation studies.



## 1. INTRODUCTION

The photoactive properties of titanium dioxide ($TiO_2$) have been utilised for two main fields of application: (i) environmental remediation including water/air purification, and selfcleaning surfaces; (ii) solar energy conversion through photoelectrolytic water splitting to yield hydrogen and oxygen [1–4]. Nanoparticle $TiO_2$ electrodes have also found application in dye sensitised photovoltaic cells [5, 6]. The reported efficiency of $TiO_2$ for solar applications in (i) and (ii) above is low due to its wide band-gap (3.0–3.2 eV) requiring ultraviolet irradiation (UV). In attempts to increase the solar efficiency by utilising visible light, $TiO_2$ has been doped with other elements with the aim of producing a red shift in the absorbance spectrum. Transition metal ions are commonly employed dopants due to their strong absorption of visible light and their similar ionic radius to the parent titanium ion. However, studies into the effectiveness of transition metal ions as dopants to improve solar efficiency have reported conflicting results. For example, chromium doping of $TiO_2$ has been reported to yield both an increase in activity [7–10] and a decrease in activity [11–16]. The majority of dopant studies do report a red shift in the absorption spectra of the doped material, however, this does not necessarily correlate with an increase in photoactivity [13, 17–20]. Unfortunately, there are few publications which report both the photocurrent response and absorption spectra for doped $TiO_2$. Where they exist, the results are conflicting, with some researchers reporting a good correlation between the photoactive spectrum and the absorption spectrum [8, 11, 17] while others have not found a correlation [21].

The direct comparison of published results for the efficiency of doped $TiO_2$ photocatalysts is not straightforward as reported materials have been produced using different methods and have been tested under different conditions. For example, if the photocatalytic degradation of a model pollutant is used as the measure of efficacy then changes in surface adsorption, due to changes in surface PZC resulting from doping, may result in an increase in photocatalytic degradation rate of certain organics but not others [15, 22].

Only a few papers discriminate between the effects of the dopant ion energy levels and the dopant ion-induced oxygen defect energy level within band structure. An oxygen defect level is introduced when the dopant has a lower valence than titanium thus leaving oxygen bonding unsatisfied and a new energy level is produced.

The effect of this induced defect level is difficult to study within a single dopant regime. Analysis of the dopant induced oxygen level within the band structure of platinised $TiO_2$ was studied by Karakitsou and Verykios using dopants of different valences to titanium [23]. Using hydrogen evolution as the measure of photoactivity, they reported that dopants with a valence greater than 4 gave higher activity, and dopants with valence less than 4 had a lower activity, as compared to the undoped $TiO_2$. The decrease in the photoactivity with dopants of valence less than 4 was attributed to an increased rate of charge carrier recombination.

The effect of oxygen defect levels in the $TiO_2$ band structure have previously been reported in literature [24, 25]. Siripala and Tomkievicz were the first to examine the effect of these defects on charge transfer at the $TiO_2$ electrolyte interface [26]. They reported that oxygen defect levels were responsible for observed photocurrent using sub-band gap illumination. The sub-band gap photocurrent was only observed between applied potentials of −0.6 V and +0.6 V (SCE). Other workers have reported the generation of oxygen defect states via plasma modification of $TiO_2$ which yielded a visible photocurrent response [27].

In this work, we report the effect of doping with transition metal ions on changes in UV/Vis absorption spectra, crystal phase, current-potential response, and spectral photocurrent response.

## 2. EXPERIMENTAL

A sol gel procedure, adapted from the work of Murakami et al. [28] using ammonium acetate as a catalyst, was used to prepare $TiO_2$ films. A solution of 0.0973 g ammonium acetate, in 0.2 $cm^3$ water/15 $cm^3$ butan-1-ol, was added dropwise to solution of 0.377 g titanium (IV) butoxide in 10 $cm^3$ butan-1-ol. For doped samples, the relevant dopant acetate salt was added along with the ammonium acetate to give 0.2, 1.0, or 5.0 atom% (with respect to titanium). Dopants investigated were V, Cr, Mn, Fe, Co, Ni, and Cu. The resulting transparent sol gel was stirred for a further 1 hour before dip coating onto previously cleaned $2 \times 2\,cm^2$ titanium foil coupons ($1.27 \times 10^{-2}$ cm thick, Aldrich). Films were deposited in five coat cycles, drying between coats with an infrared lamp, before annealing at 500°C in air for 1 hour with a temperature ramp rate 1°C $min^{-1}$. Electrical contact was made to the coupons by attaching copper wire with conductive silver epoxy (Circuit Works, Chemtronics). The contact and coupons were painted with a negative photoresist (KPR resist, Casio Chemicals) and UV cured, leaving a defined area of $TiO_2$ exposed.

Electrochemical characterisation of samples was performed under potentiostatic control (Autolab PGSTAT30) in a one-compartment cell with quartz window, platinum basket counter electrode, and a saturated calomel reference electrode (SCE). The supporting electrolyte was 0.1 M sodium perchlorate, and irradiation was provided from a 1 kW Xe arc lamp (ss1000 Spears Robinson) either; unfiltered, with an AM1 filter (to simulate solar conditions) or with a sodium nitrite filter ($\lambda > 420$ nm) for high-intensity visible light. For monochromatic irradiation, a high-intensity monochromator (GM252, set for 10 nm band pass) was positioned between the source and the photoreactor. Light intensity was measured using a calibrated spectral radiometer (Jobin Yvonne Gemini spectral radiometer). Linear sweep voltammetry (LSV) was carried scanning from –1.0 V to +1.5 V with a scan rate of 10 mV $s^{-1}$. The current-time response was measured at fixed potentials using chopped irradiation (Uniblitz vmm-t1, Vincent Associates). The cell temperature was maintained at 25°C ± 2°C. The presence or absence of dissolved oxygen was controlled by sparging with air or oxygen free nitrogen (OFN), respectively. All potentials are reported versus SCE.

Table 1: Elemental analysis by AES for Cu and Cr doped $TiO_2$ films.

| Sample | Cu doped sample 1 atom% precursor | | | |
|---|---|---|---|---|
| Element | Carbon | Oxygen | Titanium | Copper |
| Before etch | 8.65% | 75.17% | 15.79% | 0.39% |
| After etch | 22.86% | 52.42% | 24.64% | 0.09% |
| | Cr doped sample 5 atom% precursor | | | |
| Element | Carbon | Oxygen | Titanium | Chromium |
| Before etch | 13.57% | 66.60% | 17.63% | 2.20% |
| After etch | 11.44% | 66.75% | 20.21% | 1.59% |

Elemental analysis was carried out by Auger electron spectroscopy (AES) (Kratos Φ 660) in a vacuum of $10^{-6}$ torr with electrons accelerated from a field-emission source at 4 kV accelerating voltage to give a beam current of 2 $\mu$A. Depth profiling was achieved using an argon etch.

UV-Vis transmission spectra of films deposited on quartz were measured using a spectrophotometer (Lambda 11, Perkin Elmer). Optical band-gap values were calculated by extrapolation of the absorption band edge. Crystal phase was analysed by Raman spectroscopy (LabRam 300, ISA instruments) by comparing to commercial anatase (99.5%, Aldrich) and rutile (created from predominantly rutile sample (Aldrich) by heating to 800°C). The source was an argon laser $\lambda = 514$ nm. Optimum analysis was performed with an acquisition time of 5 seconds, averaged over 10 accumulations, with the neutral density filter set to 50%.

## 3. RESULTS AND DISCUSSION

AES measurements indicated that not all of the corresponding dopant was incorporated at the hydrolysis stage of sol-gel procedure. Determination of dopant concentrations at initial precursor levels below 1.0 atom% was not possible with the AES system used in this study. Analysis of doped samples containing 1.0 atom% and 5.0 atom%, as precursor, confirmed the presence of the dopants (Table 1), however, they were at much lower levels (ca. 40%) than that of the initial precursor dopant level.

For simplicity, we will continue to refer to percentage doping of samples as the initial concentration of dopant added to the sol precursor. Depth profiling of the thin films showed that the dopant species were preferentially located on the surface with lower concentrations present in the bulk. Additionally, a high proportion of carbon was measured

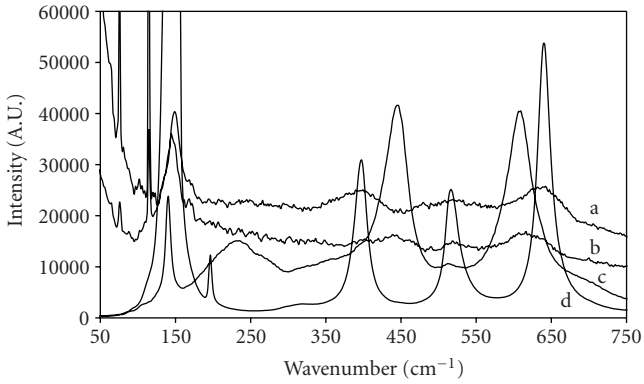


FIGURE 1: Raman spectra of (a) undoped $TiO_2$ film, (b) vanadium doped $TiO_2$, (c) commercial anatase powder, (d) commercial rutile powder (following high-temperature anneal).

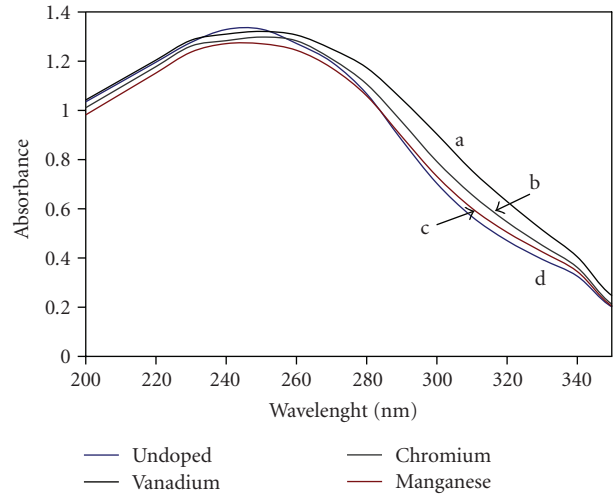


FIGURE 2: UV/Vis absorption spectra of doped $TiO_2$ films (a) V 0.2 atom%, (b) Cr 0.2 atom%, (c) Mn 0.2 atom%, (d) undoped $TiO_2$.

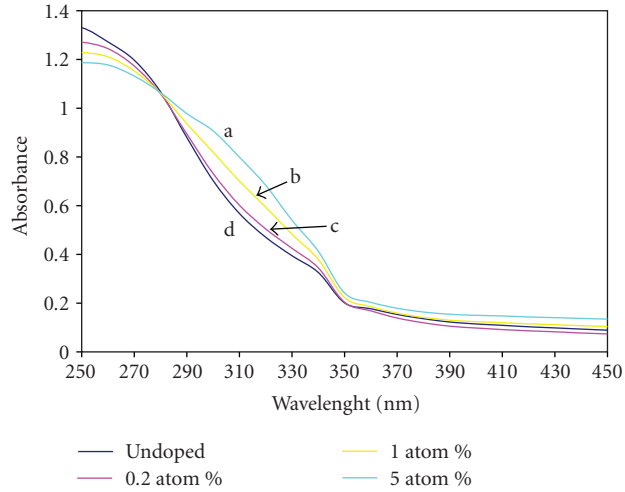


FIGURE 3: UV/Vis absorbance versus dopant concentration for $TiO_2$:Mn (a) 5 atom%, (b) 1 atom%, (c) 0.2 atom%, (d) undoped.

which originated from the alkoxide precursor used in the sol-gel process. Carbon was present in all samples including the undoped sample.

Figure 1 shows the Raman spectra obtained for a $TiO_2$ film and a $TiO_2$:V film, compared with anatase and rutile powders. Analysis of the powder samples showed all relevant Raman vibration modes of anatase and rutile correlating with previous literature on Raman analysis of $TiO_2$ [29]. Comparison of the sol-gel derived thin films showed all samples to contain the $E_g$ vibrational mode at 144 $cm^{-1}$ common to both anatase and rutile. However, the rutile signal at 144 $cm^{-1}$ is much weaker compared to the anatase signal. Since the sol-gel film shows a large peak at 144 $cm^{-1}$ but no other rutile peaks, then we can assume it was predominantly anatase. The $TiO_2$:V sample showed peaks present at 447 $cm^{-1}$ ($E_g$) and 612 $cm^{-1}$ ($A_{1g}$) representative of rutile and 519 $cm^{-1}$ ($B_{1g}$) representative of an anatase crystal structure. The spectra of the undoped sample and all other doped samples were almost identical showing a predominantly anatase crystal phase, with the 399 $cm^{-1}$ and 519 $cm^{-1}$ $B_{1g}$ peaks, along with the 639 $cm^{-1}$ $E_g$ peak associated with anatase.

UV-Vis absorption spectroscopy of the doped films, deposited on quartz, showed a minor red shift in the absorbance spectra as compared to the undoped film, however, this was mainly confined to the region from 250 nm to 350 nm (examples in Figure 2).

With all dopants investigated, an increase in the dopant concentration resulted in an increase in the absorbance between 290 nm and 350 nm with a small increase in absorbance at wavelengths greater than 350 nm. For example, the change in absorbance with concentration of dopant using $TiO_2$:Mn is given in Figure 3. Changes in the absorption band edge, obtained by extrapolation of the UV/Vis absorption data, were in the range of 0.01–0.25 eV. The error in these calculations was not acceptable and therefore we do not report the band-gap values.

The photoelectrochemical characterisation of the films using linear sweep voltammetry (LSV) showed a typical *n*-type semiconductor response with negligible anodic current in the dark and a significant increase in the anodic current under AM1 solar simulated irradiation (Figure 4).

The photocurrent was dependent on the applied potential, and the undoped $TiO_2$ sample showed a larger photocurrent response than any of the doped samples. Furthermore, a decrease in photocurrent with increasing dopant concentration was observed with all doped samples. Air sparging of the electrolyte prior to LSV resulted in a positive shift in the onset potential for anodic current (Figure 5 and Table 2).

The photocurrent response spectra of these films were obtained using chopped monochromatic illumination (10 nm band pass). The spectral current-time response for the undoped $TiO_2$ electrode is given in Figure 6. The incident photon conversion efficiency (IPCE) was calculated by

$$\%\text{IPCE} = \frac{J}{I_0 F} \times 100, \quad (1)$$

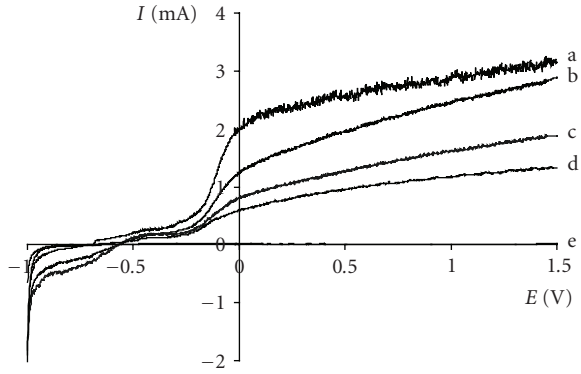


Figure 4: Linear sweep voltammograms under AM1 solar simulated irradiation for doped $TiO_2$ films (0.5 atom% dopant) (a) undoped, (b) Fe, (c) Co, (d) Ni, (e) dark response for undoped film.

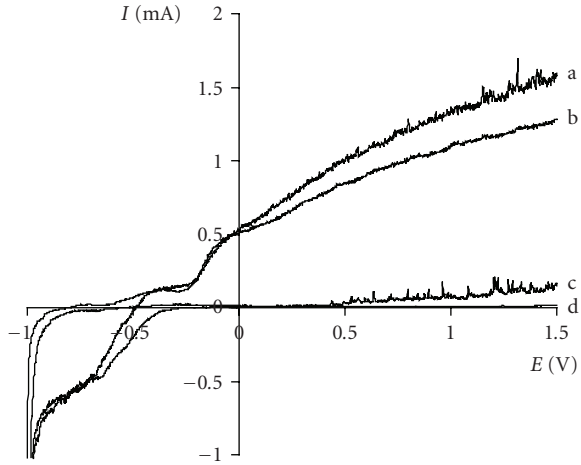


Figure 5: Effect of electrolyte air sparging on the *I-E* response for $TiO_2$:Cr (0.2 atom%) under unfiltered irradiation (a) light, following air sparging, (b) light, following nitrogen sparging, (c) dark, following air sparging, (d) dark, following nitrogen sparging (SR = 10 mV $s^{-1}$).

where $J$ is the photocurrent density, $I_0$ is the incident light intensity, and $F$ is Faraday's constant.

The %IPCE versus wavelength is given in Figure 7. The monochromatic light intensity was a limiting factor in these experiments yielding very low photocurrents. A small photocurrent response at wavelengths above 400 nm was observed for a number of samples (see Figure 6), however, a change in current less than three times the deviation of the background current (i.e., 30 nA) was not taken as significant. The doped samples exhibited no red shift in the %IPCE compared to the undoped $TiO_2$.

To overcome the limitations of the low light intensity of the monochromatic source, the photocurrent response was measured under visible excitation using a $NaNO_2$ filter ($\lambda \geq 410$ nm) with the Xe source. All samples showed a photocurrent response under sub-band gap irradiation which was dependent on applied potential with the photocurrent maxima observed between −0.5 and −0.1 V (see Figure 8).

Table 2: Anodic photocurrent onset potential for different preparations in the presence of oxygen (the undoped sample gave an onset potential of –0.8 V).

| | Onset potential (V) | | |
|---|---|---|---|
| Dopant | 0.2 atom% | 1.0 atom% | 5.0 atom% |
| Vanadium | −0.49 | −0.47 | −0.46 |
| Chromium | −0.48 | −0.48 | −0.45 |
| Manganese | −0.47 | −0.45 | −0.41 |
| Iron | −0.56 | −0.45 | −0.49 |
| Cobalt | −0.58 | −0.44 | −0.45 |
| Nickel | −0.52 | −0.49 | −0.44 |
| Copper | −0.67 | −0.56 | −0.54 |

Table 3: Photoelectrochemical data for undoped and 0.5 atom% doped $TiO_2$ films under visible irradiation.

| Dopant | Onset potential for anodic current (V) | Peak potential (V) | Photocurrent at peak potential (mA) |
|---|---|---|---|
| None | −0.71 | −0.19 | 0.038 |
| Vanadium | −0.51 | −0.24 | 0.049 |
| Chromium | −0.49 | −0.26 | 0.051 |
| Manganese | −0.53 | −0.30 | 0.070 |
| Iron | −0.51 | −0.22 | 0.044 |
| Cobalt | −0.60 | −0.31 | 0.076 |
| Nickel | −0.53 | −0.35 | 0.066 |
| Copper | −0.62 | −0.30 | 0.062 |

The peak potentials and onset potentials for anodic current are given in Table 3. AES analysis confirmed the presence of carbon impurities at high levels and this is common with sol-gel routes employing alkoxide precursors. It has been previously reported that carbon doped $TiO_2$ gives a visible response [30]. All samples contained carbon impurities and there was a small visible response observed for the *undoped* $TiO_2$ sample. This visible photocurrent for the *undoped* sample, which may be due to carbon impurities, is much less than that observed for the metal ion dopants (see Figure 8 and Table 3). Recently, Asahi et al. [31] reported the carbon defect level to be too low to give an optical transition in the visible. Changes in the optical or photoactive spectra of $TiO_2$ due carbon doping have been correlated to an increase in the concentration of $Ti^{3+}$ stabilised by carbon impurities [32, 33].

The presence of metal ion dopants will result in oxygen vacancy states or single-bonded oxygen (possibly hydroxyl) due to the lower coordination of the dopant with respect to the parent $Ti^{4+}$. Nakamura et al. [27] reported that $H_2$ plasma treatment of $TiO_2$ resulted in the formation of oxygen vacancy states located around 2.02–2.45 eV above the valence band corresponding to a wavelength between 506 and 614 nm. Electrons may be promoted from the valence band to the vacancy states by visible light excitation. They

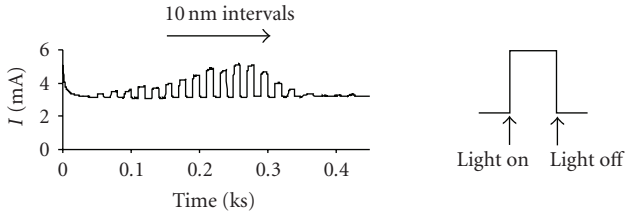


Figure 6: Current-time response under chopped irradiation for undoped sample as function of irradiation wavelength from 250 to 430 nm (left to right) in 10 nm intervals. Measured in a one-compartment cell with applied potential of +1.0 V and 0.1 M sodium perchlorate as a backing electrolyte with air sparging.

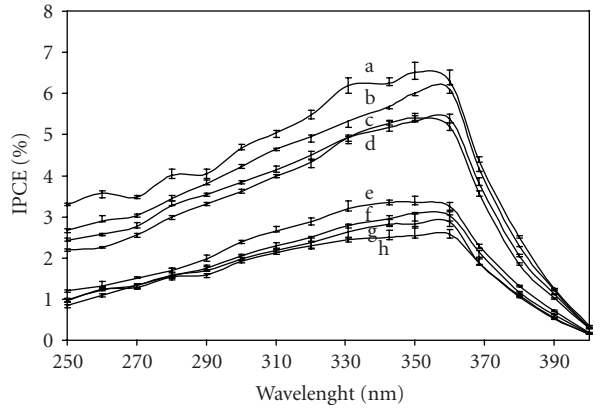


Figure 7: Incident photon to current efficiency for samples doped to 0.5 atom%. Dopant: (a) none, (b) Fe, (c) Cu, (d) V, (e) Co, (f) Cr, (g) Ni, (h) Mn (measured in a one-compartment cell at an applied potential of +1.0 V and 0.1 M sodium perchlorate electrolyte with air sparging).

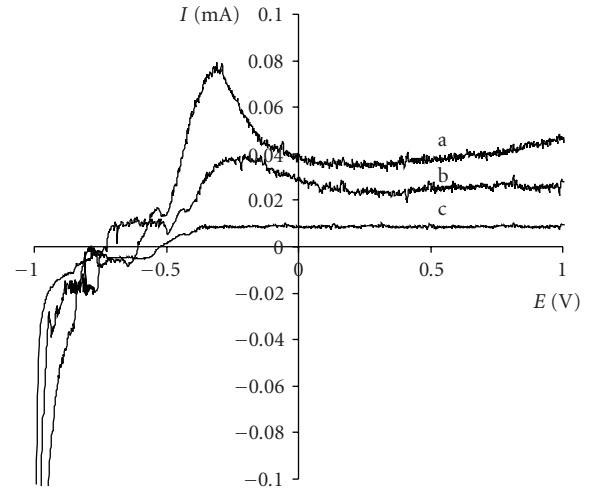


Figure 8: Visible ($\lambda > 410$ nm) photocurrent response (a) $TiO_2$:Co 0.5 atom%, (b) undoped $TiO_2$, and (c) dark current for undoped $TiO_2$.

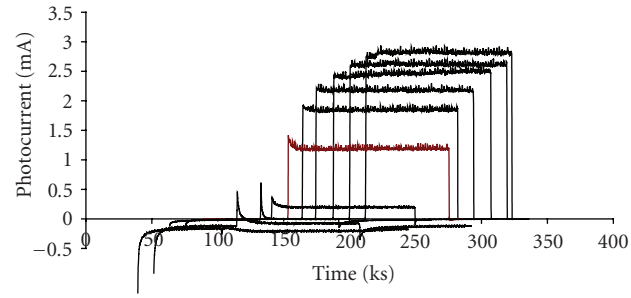


Figure 9: Changes in photocurrent transients as a function applied potential. Example of undoped sample under polychromatic illumination (applied bias from 1.0 V to −1.0 V in 0.2 V steps left to right).

reported that plasma modification of $TiO_2$ allowed visible-light-driven oxidation of NO.

Siripala and Tomkievicz [26] investigated interactions between photoinduced and dark charge transfer at single crystal $TiO_2$-aqueous electrolyte interfaces. They reported a sub-band gap irradiation resulted in electron injection from the valence band to states in the gap which lie around 0.6 eV below the bottom of the conduction band. Carrier excitation through such surface states should be much less potential dependent than carrier excitation through the bulk. Indeed they report that sub-band gap photocurrent is observed only between −0.5 and +0.4 V (SCE) at pH 6.5 (reported flat band potential was ca. −0.8 V). They proposed that the surface state was an intermediate of the dark reaction forming $TiO_2$–H, the energy for which lies within the band-gap.

The photocurrent under visible light excitation observed at negative potentials is consistent with previously published results which attribute this visible response to donor/acceptor energy levels below the conduction band caused by surface defects [24–27]. Photocurrent under sub-band gap illumination is only observed in the potential region where donor/acceptor energy levels are filled, that is, more negative than −0.1 V in this case. The presence of defect states is usually reported to have a negative effect on photoactivity because they act as recombination centres for charge carriers. However, under appropriate applied potential, these defect levels can act as electron donor states yielding a photocurrent response under sub-band gap irradiation.

To investigate the potential dependence of these defect levels, the current-time response of $TiO_2$ electrodes under chopped illumination was examined. Salvador [34] investigated the kinetics of recombination involving defects, surface groups, and absorbed species, by photocurrent transient measurements. Using single crystal $TiO_2$ electrodes, they reported that the initial photocurrent produced in the instant of illumination ($I_{ph\,in}$) decayed with time to a steady state ($I_{ph\,st}$) due to recombination on defects and surface states. By plotting the ratio of $I_{ph\,st}/I_{ph\,in}$ versus potential, the critical band bending was determined.

Figures 9 and 10 show examples of transients produced in this work for the undoped and doped samples, respectively. For the undoped samples, the initial photocurrent spike is

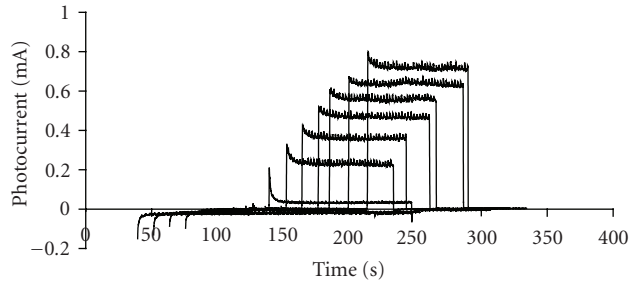


Figure 10: Changes in photocurrent transients as a function applied potential. Example of 0.2% chromium doped sample under polychromatic illumination (applied bias from +1.0 V to −1.0 V in 0.2 V steps left to right).

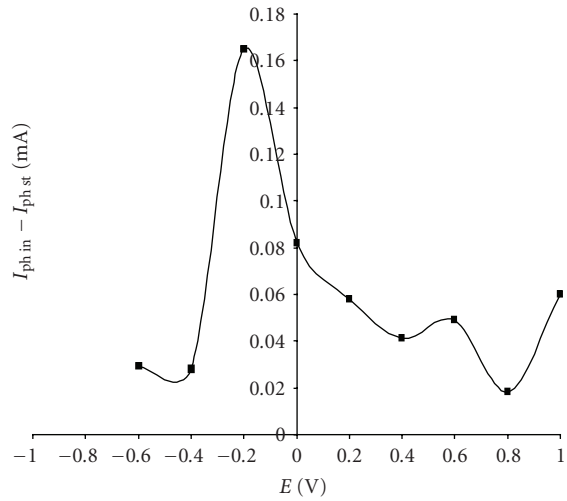


Figure 11: $I_{ph\,in} - I_{ph\,st}$ as a function of potential from 0.2 atom% chromium doped sample.

absent at potentials more positive than +0.6 V whilst for the doped samples, the initial spike was always present. Additionally, photocurrent showed *n*-type to *p*-type conversion at negative potentials close the $E_{fb}$. Matsumoto et al. [21] reported increasing *p*-type character at negative potentials following doping with transition metals which resulted in a lowering of the anodic photocurrent in comparison to the undoped sample, with higher *p*/*n* ratios correlating to higher defect densities.

The films used in this study were made using a sol-gel route which gave oxide films consisting of nanoparticles with a primary particle size around 38 nm [35]. For nanoparticles in this size range, band bending is not significant. However, initial and steady state photocurrent measurements can still be used to examine recombination as a function of potential by subtracting $I_{ph\,st}$ from $I_{ph\,in}$. Figure 11 shows the potential dependence of recombination in these electrodes. The peaks in recombination ($I_{ph\,in} - I_{ph\,st}$) with respect to potential are tabulated in Table 4.

The magnitude of $I_{ph\,in} - I_{ph\,st}$ is observed to follow the same potential dependence as the sub-band gap photocurrent response. Under band-gap irradiation, the defect states act as recombination centres lowering the photocurrent response at negative potentials; however, under sub-band gap irradiation, the defect states act as electron donors showing a visible photocurrent response. This is an agreement with other reported results [36].

Table 4: Potential dependence of recombination.

| Dopant | Peak in $I_{ph\,in} - I_{ph\,st}$ (V) |
|---|---|
| Undoped | 0.0 |
| Vanadium | −0.2 |
| Chromium | −0.2 |
| Manganese | −0.2 |
| Iron | −0.2 |
| Cobalt | −0.4 |
| Nickel | −0.4 |
| Copper | −0.4 |

There is a small visible photocurrent response is observed at potentials more positive than −0.6 V due to defect states. Nevertheless, it is clear that the primary band-gap photocurrent response is decreased by the addition of metal ion dopants, which act as charge-carrier recombination centres, and that the sub-band gap photocurrent is only a fraction of the band-gap photocurrent and, therefore, may not be relevant for practical applications including the photoelectrolytic splitting of water under solar irradiation.

## 4. CONCLUSIONS

Thin films of transition metal doped (0.2, 1.0, and 5.0 atom%) $TiO_2$ were prepared on titanium foil using a sol-gel route catalyzed by ammonium acetate. Raman spectroscopy confirmed anatase crystal phase in all samples except in the case of the $TiO_2$:V sample where a mixture of anatase and rutile was obtained.

The films doped with transition metal ions showed lower photocurrent response than undoped samples under simulated solar irradiation. The photocurrent response spectra of the doped films were similar to the undoped sample with no major red shift. Sub-band gap irradiation of the samples gave a small photocurrent at negative potentials which is indicative of electron promotion from a filled defect level, the occupation of which is potential dependant. Examination of defect level potential dependence by analysis of photocurrent transients (from −0.8 to +1 V) showed a good correlation with the potential dependence in visible illumination studies.

The primary band-gap photocurrent response is decreased by the addition of metal ion dopants, which act as charge-carrier recombination centres, and the sub-band gap photocurrent is only a very small fraction of the band-gap photocurrent.

## ACKNOWLEDGMENT

Department of Employment and Learning Northern Ireland for funding JWJ Hamilton.

## REFERENCES


[1] A. Mills, R. H. Davies, and D. Worsley, "Water purification by semiconductor photocatalysis," *Chemical Society Reviews*, vol. 22, no. 6, pp. 417–425, 1993.

[2] R. J. Watts, S. Kong, M. P. Orr, G. C. Miller, and B. E. Henry, "Photocatalytic inactivation of coliform bacteria and viruses in secondary waste-water effluent," *Water Research*, vol. 29, no. 1, pp. 95–100, 1995.

[3] O. Legrini, E. Oliveros, and A. M. Braun, "Photochemical processes for water treatment," *Chemical Reviews*, vol. 93, no. 2, pp. 671–698, 1993.

[4] A. Mills, A. Lepre, N. Elliott, S. Bhopal, I. P. Parkin, and S. A. O'Neill, "Characterisation of the photocatalyst Pilkington Activ$^{TM}$: a reference film photocatalyst?" *Photochemistry and Photobiology A*, vol. 160, no. 3, pp. 213–244, 2003.

[5] B. O'Regan and M. Grätzel, "A low cost, high efficiency solar cell based on dye sensitised colloidal $TiO_2$ films," *Nature*, vol. 353, no. 6346, pp. 737–740, 1991.

[6] M. Grätzel, "Photovoltaic and photoelectrochemical conversion of solar energy," *Philosophical Transactions of the Royal Society A*, vol. 365, no. 1853, pp. 993–1005, 2007.

[7] E. Borgarello, J. Kiwi, M. Grätzel, E. Pelizzetti, and M. Visca, "Visible light induced water cleavage in colloidal solutions of chromium-doped titanium dioxide particles," *Journal of the American Chemical Society*, vol. 104, no. 11, pp. 2996–3002, 1982.

[8] M. Anpo, "Photocatalysis on titanium oxide catalysts: approaches in achieving highly efficient reactions and realizing the use of visible light," *Catalysis Surveys from Japan*, vol. 1, no. 2, pp. 169–179, 1997.

[9] Y. Wang, H. Cheng, Y. Hao, J. Ma, W. Li, and S. Cai, "Photoelectrochemical properties of metal-ion-doped $TiO_2$ nanocrystalline electrodes," *Thin Solid Films*, vol. 349, no. 1-2, pp. 120–125, 1999.

[10] W. Choi, A. Termin, and M. R. Hoffmann, "The role of metal-ion dopants in quantum-sized $TiO_2$: correlation between photoreactivity and charge carrier recombination dynamics," *Journal of Physical Chemistry*, vol. 98, no. 51, pp. 13669–13679, 1994.

[11] A. Monnier and J. Augustynski, "Photoelectrolysis of water: photoresponses of nickel, chromium and zinc-doped polycrystalline $TiO_2$ electrodes," *Journal of the Electrochemical Society*, vol. 127, no. 7, pp. 1576–1579, 1980.

[12] Z. H. Luo and Q.-H. Gao, "Decrease in the photoactivity of $TiO_2$ pigment on doping with transition-metals," *Journal of Photochemistry and Photobiology A*, vol. 63, no. 3, pp. 367–375, 1992.

[13] H. Wittmer, St. Holten, H. Kliem, and H. D. Breuer, "Detection of space charge limited currents in nanoscaled titania," *Physica Status Solidi (A)*, vol. 181, no. 2, pp. 461–469, 2000.

[14] V. Brezová, A. Blažková, L. Karpinský, et al., "Phenol decomposition using $M^{n+}/TiO_2$ photocatalysts supported by the sol-gel technique on glass fibres," *Journal of Photochemistry and Photobiology A*, vol. 109, no. 2, pp. 177–183, 1997.

[15] A. Di Paola, E. García-López, S. Ikeda, G. Marcì, B. Ohtani, and L. Palmisano, "Photocatalytic degradation of organic compounds in aqueous systems by transition metal doped polycrystalline $TiO_2$," *Catalysis Today*, vol. 75, no. 1–4, pp. 87–93, 2002.

[16] J. A. Navío, J. J. Testa, P. Djedjeian, J. R. Padrón, D. Rodríguez, and M. I. Litter, "Iron-doped titania powders prepared by a sol-gel method—part II: photocatalytic properties," *Applied Catalysis A*, vol. 178, no. 2, pp. 191–203, 1999.

[17] T. E. Phillips, K. Moorjani, J. C. Murphy, and T. O. Poehler, "$TiO_2$-$VO_2$ alloys—reduced bandgap effects in the photoelectrolysis of water," *Journal of the Electrochemical Society*, vol. 129, no. 6, pp. 1210–1215, 1982.

[18] W. Choi, A. Termin, and M. R. Hoffmann, "Effects of metal-ion dopants on the photocatalytic reactivity of quantum-sized $TiO_2$ particles," *Angewandte Chemie International Edition in English*, vol. 33, no. 10, pp. 1091–1092, 1994.

[19] A. Di Paola, G. Marcì, L. Palmisano, et al., "Preparation of polycrystalline $TiO_2$ photocatalysts impregnated with various transition metal ions: characterization and photocatalytic activity for the degradation of 4-nitrophenol," *Journal of Physical Chemistry B*, vol. 106, no. 3, pp. 637–645, 2002.

[20] D. Dvoranová, V. Brezová, M. Mazúr, and M. A. Malati, "Investigations of metal-doped titanium dioxide photocatalysts," *Applied Catalysis B*, vol. 37, no. 2, pp. 91–105, 2002.

[21] Y. Matsumoto, J.-I. Kurimoto, T. Shimizu, and E.-I. Sato, "Photoelectrochemical properties of polycrystalline $TiO_2$ doped with 3d transition-metals," *Journal of the Electrochemical Society*, vol. 128, no. 5, pp. 1040–1044, 1981.

[22] K. Wilke and H. D. Breuer, "The influence of transition metal doping on the physical and photocatalytic properties of titania," *Journal of Photochemistry and Photobiology A*, vol. 121, no. 1, pp. 49–53, 1999.

[23] K. E. Karakitsou and X. E. Verykios, "Effects of altervalent cation doping of $TiO_2$ on its performance as a photocatalyst for water cleavage," *Journal of Physical Chemistry*, vol. 97, no. 6, pp. 1184–1189, 1993.

[24] V. N. Bogomolov, E. K. Kudinov, D. N. Merlin, and A. Y. Frisov, "Polaron mechanism of light absorption in rutile crystals," *Soviet Physics—Solid State*, vol. 9, pp. 1630–1639, 1963.

[25] E. K. Kudinov, D. N. Mirlin, and A. Y. Firsov, "Polaron nature of the current carriers in rutile $TiO_2$," *Soviet Physics—Solid State*, vol. 11, pp. 2257–2266, 1970.

[26] W. Siripala and M. Tomkievicz, "Interactions between photoinduced and dark charge transfer across n-$TiO_2$-aqueous electrolyte interface," *Journal of the Electrochemical Society*, vol. 129, no. 6, pp. 1240–1245, 1982.

[27] I. Nakamura, N. Negishi, S. Kutsuna, T. Ihara, S. Sugihara, and K. Takeuchi, "Role of oxygen vacancy in the plasma-treated $TiO_2$ photocatalyst with visible light activity for NO removal," *Journal of Molecular Catalysis A*, vol. 161, no. 1-2, pp. 205–212, 2000.

[28] Y. Murakami, T. Matsumoto, and Y. Takasu, "Salt catalysts containing basic anions and acidic cations for the sol-gel process of titanium alkoxide: controlling the kinetics and dimensionality of the resultant titanium oxide," *Journal of Physical Chemistry B*, vol. 103, no. 11, pp. 1836–1840, 1999.

[29] Y.-H. Zhang, C. K. Chan, J. F. Porter, and W. Guo, "Micro-Raman spectroscopic characterization of nanosized $TiO_2$ powders prepared by vapor hydrolysis," *Journal of Materials Research*, vol. 13, no. 9, pp. 2602–2609, 1998.

[30] S. Sakthivel and H. Kisch, "Daylight photocatalysis by carbon-modified titanium dioxide," *Angewandte Chemie International Edition*, vol. 42, no. 40, pp. 4908–4911, 2003.

[31] R. Asahi, T. Morikawa, T. Ohwaki, K. Aoki, and Y. Taga, "Visible-light photocatalysis in nitrogen-doped titanium oxides," *Science*, vol. 293, no. 5528, pp. 269–271, 2001.

[32] Y. Li, D.-S. Hwang, N. H. Lee, and S.-J. Kim, "Synthesis and characterization of carbon-doped titania as an artificial solar light sensitive photocatalyst," *Chemical Physics Letters*, vol. 404, no. 1–3, pp. 25–29, 2005.

[33] X.-Q. Chen, H.-B. Liu, and G.-B. Gu, "Preparation of nanometer crystalline $TiO_2$ with high photo-catalytic activity by pyrolysis of titanyl organic compounds and photo-catalytic mechanism," *Materials Chemistry and Physics*, vol. 91, no. 2-3, pp. 317–324, 2005.

[34] P. Salvador, "Kinetic approach to the photocurrent transients in water photoelectrolysis at n-$TiO_2$ dioxide electrodes—1: analysis of the ratio of the instantaneous to steady-state photocurrent," *Journal of Physical Chemistry*, vol. 89, no. 18, pp. 3863–3869, 1985.

[35] J. W. J. Hamilton, "Preparation and characterisation of photo-anode materials," Ph.D. thesis, Faculty of Engineering, University of Ulster, Northern Ireland, UK, 2004.

[36] N. Beermann, G. Boschloo, and A. Hagfeldt, "Trapping of electrons in nanostructured $TiO_2$ studied by photocurrent transients," *Journal of Photochemistry and Photobiology A*, vol. 152, no. 1–3, pp. 213–218, 2002.